THERMAL MODELING AND ANALYSIS OF AN ON-BOARD INTERNAL-COMBUSTION-ENGINE-BASED POWERTRAIN

Abdelraouf Mayyas, Arizona State University; Mohammad Omar, Clemson University; Pierluigi Pisu, Clemson University;
A. M. Kannan, Arizona State University

Abstract

In this study, the authors developed a three-dimensional (3D) thermal model of an internal-combustion-engine-propelled powertrain using a Finite Element (FE) analysis complemented with experimentally extracted boundary conditions. The experimental work included full-field and discrete temperature measurements of an engine-based powertrain system under a wide range of road loads (vehicle speed and road grades). This paper presents a complete analysis of an inline 6-cylinder, 3.0L, 255hp powertrain's thermal characteristic and its relationship to vehicle speed and road loads. This study adopted the approach of combining both simulation and experiment in order to determine the time-dependent boundary conditions, heat sources and heat sinks in a powerful thermal-solver "RadTherm". The proposed 3D thermal model was used to perform transient and steady-state thermal analyses. A four-wheel-drive (4WD) chassis dynamometer was used to implement various driving scenarios during testing, while a network of thermo-couples and a micro-bolometric detector were used to acquire the temperature maps. The results of the thermal analysis from the model were compared with experimental results to provide a valuable conclusion. The developed model was also further utilized to optimize thermal packaging design of some powertrain parts through, but not limited to, rerouting of the heat sources and heat sinks in the vehicle design, applying thermal shields, replacing materials and increasing cooling.

Introduction

Recent governmental regulations pressing for improved fuel economy in terms of miles per gallon (MPG)—e.g., the CAFÉ standards—forced automakers to revisit and further improve their vehicular thermal management systems. At the same time, current studies of the vehicular thermal management systems still rely on simulating the heat transfer of as-built automotive parts using a Computer Aided Design (CAD) tool to describe the geometries and topologies, followed by a Computational Fluid Dynamics (CFD) tool to solve the heat transfer equations. Typically, thermal modeling assists in analyzing thermal loads of underhood components for better thermal packaging schemes that might lead to reductions in exhaust emissions and an increase in thermal efficiency. In addition, new packaging concepts might also result in weight and cost savings, and might allow engineers to devise new control strategies for cooling. Such new strategies might include electrically driven cooling systems or the use of materials with improved thermal properties. This paper describes the development of a 3D Finite Element (FE) thermal model for an internal-combustion-engine -propelled powertrain along with its exhaust system components.

Literature Review

Several vehicle thermal models have focused on investigating vehicular underhood components; Fluent Inc. developed a comprehensive simulation tool for underhood thermal management [1] with the aim of analyzing thermal performance and characteristics of the automobiles' different underhood packaging designs. A dual-cell heat exchanger model was used to simulate the underhood non-uniform heat rejections at different ambient temperatures. However; a uniform temperature map was assumed at the exhaust manifold surface, while assuming that the exhaust pipes were the heat source. Furthermore, in this study, the 3D model surface domain was discretized using a tetra-mesh scheme, which—depending on the solver scheme used to solve the heat conduction and radiation equations—may result in non-uniform element local heat conduction.

Additionally, other commercial CFD simulations might suffer in terms of accuracy because they incorporate several assumptions and approximations, due to the fact that results for a given simulation might be applied as a boundary condition for the next run, and/or basic thermodynamic calculations or ideal cycles might be used for the sub-models. Priya et al. [2] presented a thermal model of as-built automotive parts using a software platform, MuSES, with a set of thermographic detectors for extracting the needed boundary conditions. This study focused only on the engine under idling conditions; no other loading schemes were applied. Andreas et al. [3] discussed the use of a reverse-geometry approach using thermal acquisitions from thermography to

model the vehicle components as 3D topologies, which would be used in the FE model. However, these acquired thermal maps were not 3D scans of a real-world object, but were instead surface fabrics derived from the thermal images. These thermal images, or thermograms, should first be corrected for lateral heat conduction and emissivity and material variations. Moreover, such thermal images provide a surface fabric without representing a precise surface geometrical shape, especially when intricate geometries are involved. Omar et al. [4] introduced an approach to correct the thermograms for lateral heat conduction and emissivity effects using a Thermal Point Spread Function (T-PSF) and emissivity maps, respectively.

Methodology

Understanding the boundary conditions for the underhood components is vital to be able to guarantee modeling accuracy; hence, in this study, a set of thermographic detectors were employed in order to capture the underhood components' boundary conditions under different road load conditions. The infrared detectors, with their contactless, real-time temperature measurement capability, can provide accurate temporal and spatial temperature maps, when corrected for emissivity and environment contributions [5], [6]. This study employed two different thermal imagers: 1) a micro-bolometric focal plane array operating in the Long Wave Infrared LWIR 8–13 micron spectra; and, 2) a cooled, Indium Antimonite InSb detector with sensitivity in the Mid-Wave MWIR 3–5 spectra.

To mimic the different road loads and driving conditions under the controlled environment, a 4-wheel-drive, 4-roller chassis dynamometer (Renk Labeco, 500HP) was used along with a 500HP FEV engine dynamometer. The test vehicle in this study was a BMW 35i with a 6-cylinder in-line, 3.0L, 255HP engine.

The uncooled micro-bolometric detector (commercial name A40M, a product of FLIR Systems, Inc.) is capable of a 33Hz acquisition rate with a resolution of 1.3mrad, and a thermal sensitivity of 0.08C^{o} at 30C^{o}. It is capable of detecting a temperature range from -40C^{o} to 500C^{o} with an accuracy of 2% or 2C^{o}. The cooled detector is a Phoenix DTS package able to acquire up to 20kHz with the sub-window option; its Noise Equivalent Temperature Difference (NETD) is 0.1mK. The two-camera system was used to neutralize the emissivity effects using the multi-color pyrometery calculations. Additionally, a network of thermocouples was deployed to acquire a reference temperature signal to help correct the detectors' readings. Figure 1 illustrates the experimental setup of the vehicle inside the chassis dynamometer chamber. The acquired boundary conditions were then deployed into a finite differencing code environment for thermal analysis. The 3D CAD model for the test vehicle was constructed from actual 3D scans of the objects using a stereo-based, hand-held scanner (with a resolution of 0.05mm and a depth of field of 300mm) and a Zeiss full-size Coordinate Measuring Machine CMM (commercial name Zeiss Pro-T). The surface geometries were first acquired in a stereo-lithographic (.STL) CAD file. Then, it was post-processed through rapid-forming to reverse-engineer the CAD file into each target's dimensional features, which were then meshed.

Figure 1. Renk Labeco Chassis Dynamometer

Experimental Procedures

The engine's thermal maps were monitored under various power demands at the wheels, while the chassis dynamometer was used to simulate the representative road loads (i.e., vehicle speed and road grades) by controlling wheel resistance. The infrared detectors were set up to measure the surface temperature profiles for the engine, the exhaust manifold, the catalytic converter and the muffler. These specific components were thought to represent the main heat sources under the hood and under the body. Each thermal imager field was adjusted to cover the target locations for each run, in addition to removing all of the non-value-added features or background contributions through software or hardware filters. In addition, within each Field of View (FoV), a set of Regions of Interests (ROIs) were initiated in order to collect the maximum, minimum and average temperatures to improve the acquisition accuracy. In some instances, the un-cooled detector's dynamic range was adjusted in order to capture the target peak temperature [7], [8]. Figure 2 displays the configuration of the detectors during the underhood testing.

Figure 2. Infrared Detector Setup While Detecting the Heat Emissions from Under the Hood

The thermocouples network employed a high-speed, 8-channel Thermo Couple Interface Card (TCIC) with the I/O set up through a high-speed USB interface; the TCIC DAQ was calibrated with the sample rate adjusted to 10Hz. Figure 3 shows the thermocouples mounted using an epoxy bonding agent on the catalytic converter surface.

Figure 3. Thermocouple Mounted using an Epoxy Bonding Agent on the Surface of the Catalytic Converter

Testing Behavior

The main heat source in a conventional (internal combustion propelled) vehicle is its engine, with the generated heat raising the temperature of the underhood structural components. Thus, the engine and the exhaust system—including the exhaust manifold, the catalytic converter and the muffler—were targeted in the boundary condition extraction process.

The surface temperatures for each part were captured over a 42-minute period during which the vehicle speed was set to increase by 10MPH every six minutes up to a final speed of 70MPH. However, to ensure that the test included applying representative combinations of road loads, i.e., speed and grade, the temperature acquisition tests were repeated for the grades of 3, 6, 9 and 12%, with an external draft of airflow applied to prevent engine overheating. Table 1 illustrates the vehicle speed and the associated cooling air flow rates in Cubic Foot per Minute (CFM) as applied during the test. Table 2 shows the road grades applied in each run.

Table 1. Vehicle Speeds and Associated Airflow Applied for Cooling

Load Interval	0-6	7-12	13-18	19-24	25-30	31-36	37-42
Speed	10	20	30	40	50	60	70
Air flow (cfm)	4500	4500	4500	4500	9000	9000	9000

Subsequently, the experimental data included all of the transient temperature curves from the thermocouples and the 2D spatial thermal images from the thermal cameras for each test run.

Table 2. Road Grade (%) Applied in the Test

Capture No.	I	II	III	IV
Grade %	3	6	9	12

3D Thermal Model Design

This section describes the development of the 3D FE model for the complete conventional vehicle powertrain. The current investigation utilized a Finite Differencing platform (commercial name RadTherm, product of Thermo-Analytics) as the main solver. This code included an optimized thermal solver that can provide an image viewer in wireframe, in addition to an animated thermal display [9-11]. Additionally, the RadTherm solver has the capability to address steady-state and transient scenarios. Also, the code has a 3D graphic editor to allow the user to define material properties for each of the geometrical elements or group of elements. Following the properties assignment, the solver discretizes the element for each part by breaking them into thermal nodes [12].

Since radiation is a dominant mode of heat transfer, and since the underhood geometry is rather complicated, some modeling tools may combine assumptions and proximity for

radiation. The RadTherm solver, on the other hand, delivers a complete temperature distribution and heat rates for radiation. The net radiation heat exchange between two different surfaces can be computed using Equation (1) [11]:

$$Q_{net} = A_1 F_{1-2} \sigma (T_1^4 - T_2^4) \quad (1)$$

where T_1 and T_2 are the surface temperatures in K; F_{1-2} is the view factor; A is area m^2; and, σ is the Stefan-Boltzmann constant $Wm^{-2}K^{-4}$. View factor, F_{ij} , is defined in Equation (2) [2]:

$$F_{ij} = \frac{1}{A_i} \int_{A_i} \int_{A_j} \frac{\cos\theta_i \cos\theta_j}{\pi R^2} dA_i dA_j \quad (2)$$

where A_i and A_j are the areas of the surfaces i and j, respectively, and θ_i and θ_j are the angles between the position-dependent normal vectors to surfaces i and j and a line of length R connecting the points of the normal.

For accurate radiation heat transfer, the mesh quality of the CAD model was a crucial part of this model. The FE model was constructed in this study using deployed elements with an aspect ratio (width-to-length ratio) less than 4; and, in order to guarantee the uniformity of lateral heat conduction between the connected vertices within the each element, only Tri's or Quads were used with element sizes that ranged from 5–25mm. This size range was enough to resolve the thermal spatial geometry, yielding high convergence criteria at lower tolerances [9].

Other mesh quality issues were also improved by taking into consideration connectivity, duplicate, overlapping and penetrating criteria of the radiated elements. Figure 4 shows the principal quality of the required mesh used in this model.

Figure 5 displays the 3D vehicle model. The multi-layer materials for each part can be represented theoretically by a grid of nodes, spatially defined within the same part. In this study, user thermal nodes were established in order to link the fluid streams to their bounding parts. Figure 6 shows the fluid nodes used to link the exhaust gas fluid streams to the backside of the exhaust manifold ports through the exhaust tail pipe.

The design of this model required that the heat sources in the model be defined; in other words, the experimentally obtained exhaust gas temperature curve was assigned, which represented the exhaust gas upstream inside the cylinders in a way that would simulate the combustion process inside the cylinder. Knowing that this fluid is linked with a thermal node to the back (inner) side of the cylinder block (specifically the combustion chamber) was required in order to predict the exhaust gas temperature curve experimentally. Consequently, and in order to predict the exhaust gas temperature, the exhaust gas temperature curves inside the exhaust manifold ports were predicted using the experimental data measurements.

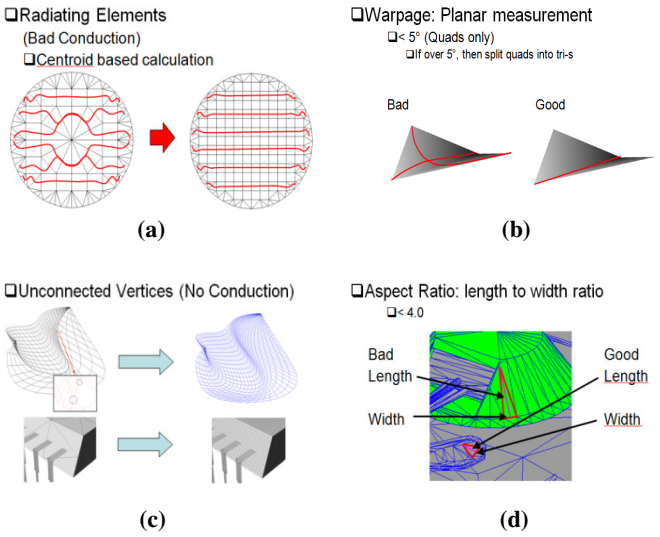

Figure 4. Meshing Requirements (a) Centroid (b) Vertices (c) Warpage (d) Aspect Ratio [9]

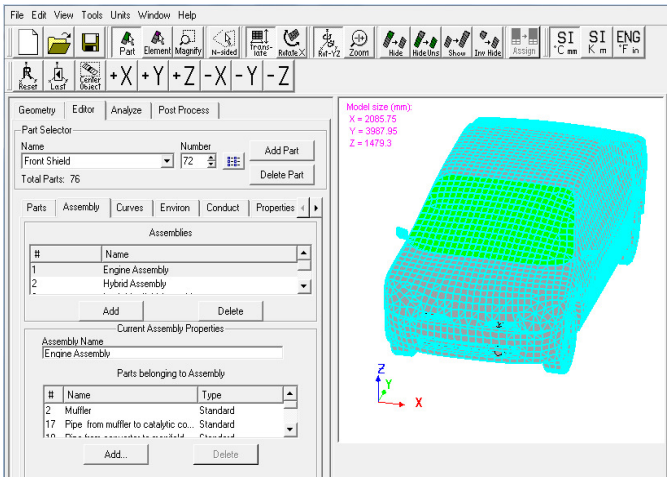

Figure 5. RadTherm Graphical User Interface

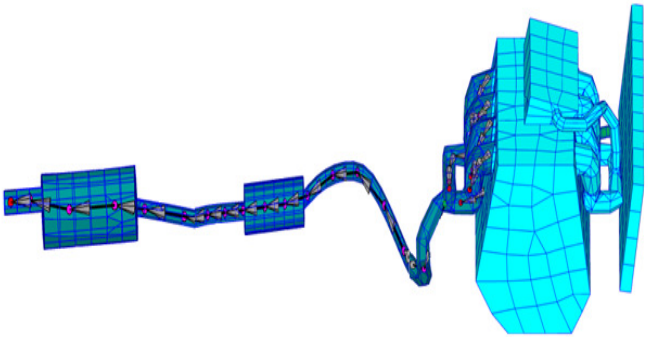

Figure 6. Exhaust Gas Fluid Streams Bounded by Exhaust System Components

The ambient air surrounding the underhood area and the underbody components was also considered in the model; a fluid node (ambient air) with an initial room temperature as recorded by the experiments was linked to the parts' front (outer) side. Finally, the lubrication and the cooling systems were simulated as a group of internal gaps created inside the cylinder block FE model; the lubricant and coolant fluid flow through these designed paths. This was done to simulate the heat rejections through these two fluids, which also aids in capturing the thermal performance of the cooling system. The coolant was then forced to circulate in and out of the cylinder block inner shell and pass through the coolant radiator. In setting up the boundary conditions process, the only assigned temperature curves were those for fluid nodes to simulate the combustion process inside each combustion chamber. These time-dependent temperature curves were synchronized with the combustion process occurrences, as obtained from the engine RPM. The exhaust gas fluid stream through the exhaust system towards the tail pipe was linked to the combustion chamber fluid nodes. The rest of the boundary conditions included an initial temperature assignment for all parts of the model.

Finally, after all boundary conditions were set up, the model was executed for all of the test runs implemented in the chassis dynamometer under the prescribed loading schemes. The model was run in 1-minute time steps, while the tolerance slope was set to a minimum. Then, the temperature curves for the different parts in the powertrain were extracted and compared against the experimental data.

Results and Discussion

The accuracy of the proposed 3D thermal model was analyzed by comparing its predicted temperature curves (spatial and transient) against the experimental data. The main goal of this simulation model was to predict the thermal signature of the underhood and underbody components under different loading profiles in terms of road loads which included vehicle speed and road grades. Figure 7 illustrates the rise in the average surface temperature for the exhaust manifold, as recorded by the un-cooled infrared detector. One can observe the high rise in temperature over time, which might lead to pixel saturation at certain temperature range settings—an integration time of the Focal Plane Array. Also, it was noticed that the components' surface temperatures increased with an increase in vehicle speed, as compared to an increase in road grade. In other words, vehicle speed causes more thermal load on the powertrain than does road grade. For instance, an increase in speed from 0–70MPH leads to a rise in exhaust manifold surface temperature to about 553K for the same 3% grade over 42 minutes. However, an increase in the grade from 3% to 12% causes an increase of only 140K in the surface temperature over the same period.

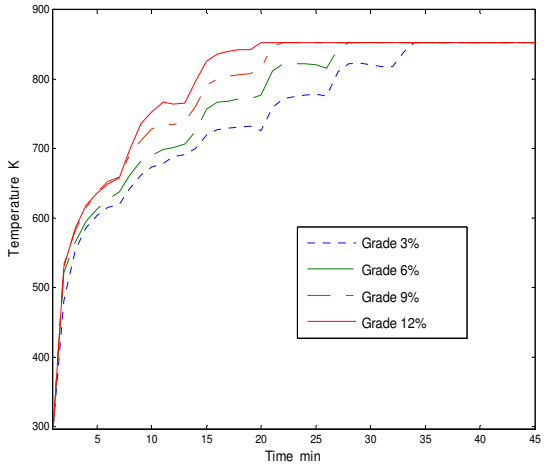

Figure 7. Exhaust Manifold Surface Temperature Curves as Recorded by the Infrared Detector

The parts' surface temperatures were plotted as a function of load; e.g., vehicle speed and road grade, as shown in Figure 8. Figure 9 illustrates the exhaust manifold surface temperature as predicted by the model in comparison with the actual temperature for the 3% and 9% road grades; the two curves were in agreement up to the point where the pixels of the infrared detector reached the saturation point. The temperature curve for the exhaust manifold surface indicated that this saturation took place after 28 and 34 minutes for road grades of 6% and 9%, respectively.

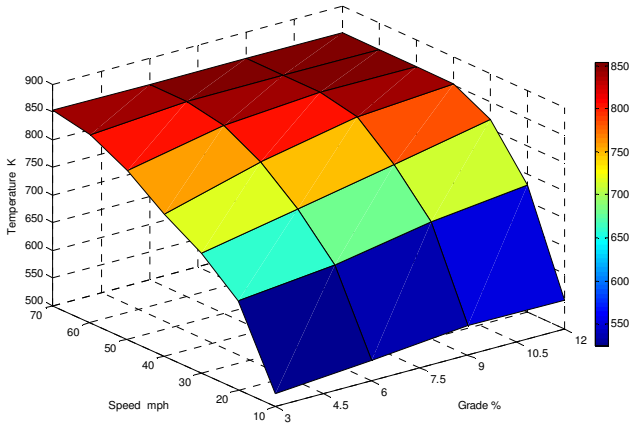

Figure 8. Exhaust Manifold Actual Surface Temperature Obtained by the Infrared Detector

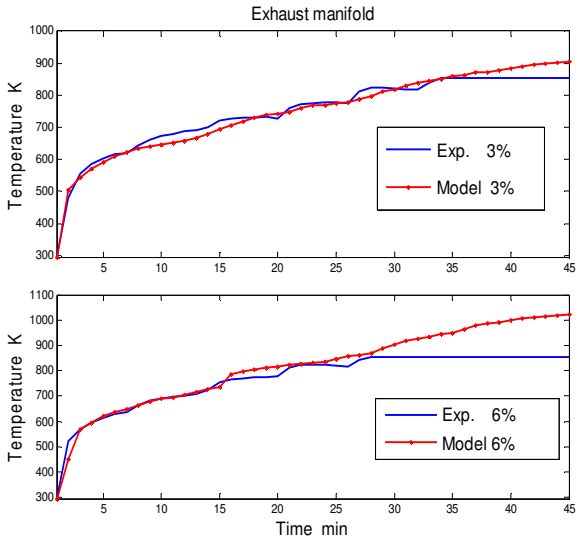

Figure 9. Exhaust Manifold Surface Temperatures as Predicted by the Model versus Actual for 3% and 6% Road Grades

In order to measure the uncertainty associated with the temperature measurements, an uncertainty analysis of both thermocouples and IR detector measurements were conducted. The input signal from the thermocouples was within the range of 0-500mV with a resolution of 0.019. The accuracy of the thermocouple acquisition was found to be ±1.5Cº. With automatic emissivity correction and a thermal sensitivity of 0.08Cº, the accuracy of the infrared detector was found to be ± 2Cº.

Subsequent to model validation, the model was utilized in optimizing the powertrain components' thermal design; several design manipulations can be tested in order to obtain better thermal performance in terms of heat rejection or insulation. These manipulations included material replacement, rerouting heat sources and heat sinks, shielding, apply different cooling at specific locations and/or load conditions, among others [13]. Consequently, several possible changes were implemented in the model; Table 3 summarizes these design modifications.

Table 3. Modifications Applied to the Current Design

Part	Current design	New design
Under Body	Steel	Aluminum, Magnesium
Engine Cylinder Block	Steel	Aluminum and Magnesium
Splash Wall	Steel	Titanium, Aluminum
Catalytic Converter	Un-shielded	Apply shielding

The automobile underbody—like other Body-in-White "BiW" panels—was made of several steel grades; at the same time, many automakers tried to replace the steel with other less dense materials such as aluminum and/or Poly-Metal Hybrids (PMH) for light-weight engineering purposes, which in turn affects the vehicle's thermal signature and impacts its thermal management system [14]. The modifications from Table 1 were implemented in the model with their thermal characteristics captured and then analyzed. For instance, Figure 10 displays the physical heat flux for a steel underbody, compared with that from an aluminum underbody. The results show that more heat is conducted through aluminum because of the higher thermal diffusivity, which allows for more heat to be rejected to the surrounding air.

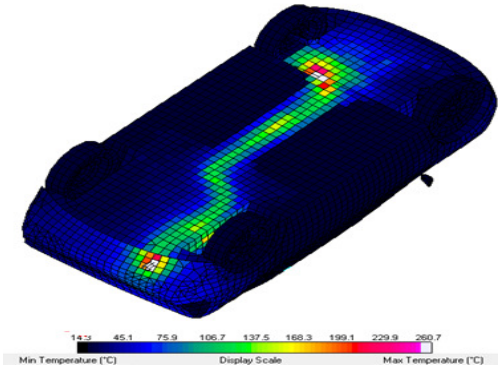

(a)

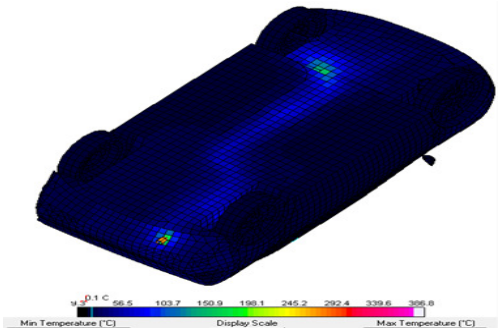

(b)

Figure 10. Heat Flux Through the Underbody: (a) Al 5083 (b) Mild Steel

Nevertheless, other packaging and thermal utilization strategies might also assist in optimizing the vehicle's thermal management system and/or its thermal signature. For example, rerouting heat sources and sinks in the vehicle might disturb the thermal management system, but packaging techniques such as applying selective shielding between the heat sources and other components can reduce the load on the underhood, temperature-sensitive components and

enhance their thermal performance; such techniques will assist in applying fewer thermal loads on specific components with sensitivity to temperature such as the electronics and the electric machines' wiring network. Also, shielding with different reflectivity grades can be tested. An test run showed how the model can predict shielding performance in preventing heat emitted by the exhaust system (see Figure 11) from being transferred into the underbody packaged components, such as the battery packs in hybrid vehicles. Nonetheless, this also assists in the improvement of the in-cabin passenger thermal comfort.

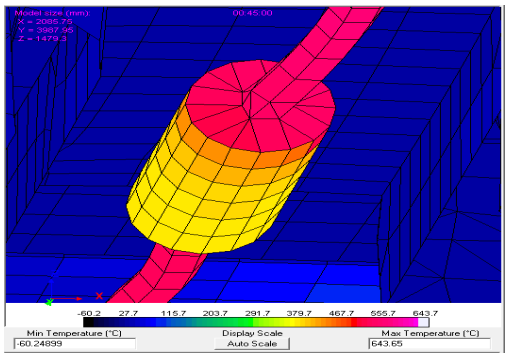

(a)

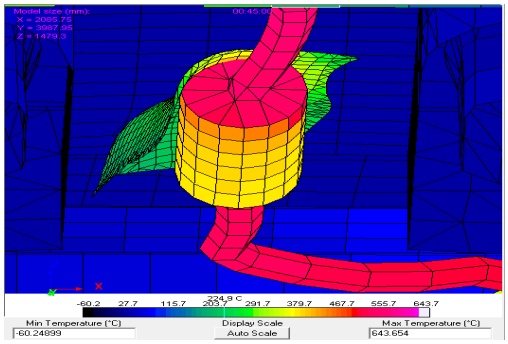

(b)

Figure 11. Heat Flux within the Catalytic Converter (zoomed): (a) Shielded (b) Un-shielded

Conclusions

This study developed a 3D FE-based model for an internal-combustion-engine-propelled vehicle, with a focus on its underhood and underbody components. The study utilized an in-house experimental setup that tested the powertrain using a 4WD chassis and engine dynamometers, in addition to using full-field and discrete-temperature measurement approaches using infrared imagers and a thermocouple network. The tests tried to imitate different road loads by changing the road grades and speed combinations for the powertrain. The 3D model utilized a multi-heat transfer and one-dimensional fluid-flow commercial thermal solver that can assign fluid streams and thermal nodes of the components' CAD surface geometries, while linking all of the model parameters to simulate actual conditions. The results showed that the results from the model are in agreement with experimental results. Also, the results exposed the effect of vehicle speed and road grade on the exhaust system thermal loads, further showing that speed has a bigger impact. Additionally, the study showed the potential of the developed model in testing different design concepts in terms of shielding characteristics and vehicle powertrain thermal repackaging.

References

[1] Application series from Fluent, (2003, June). *Under Hood Thermal management*. Fluent Inco, EX201-2003.

[2] Govindasamy, V. P. M. (2004), *Thermal Modeling and Imaging of As-built Automotive Parts*. Thesis, University of Tennessee, Knoxville.

[3] Koschan, A. F., Govindasamy, P., & Sreeenivas, S. (2006). Thermal Modeling and Imaging of as-Built Vehicle Components. *SAE* 2006-01-1167.

[4] Omar, M. A. (2010). *Dedicated processing routines for industrial thermograms*. (1st ed.). Wiley.

[5] Zhou, Y., Mayyas, A., & Omar, M. A. (2011). Principal Component Analysis-Based Image Fusion Routine with Application to Automotive Stamping Split Detection. *Research in Nondestructive Evaluation, 22*, 76-91.

[6] Korukçu, M. Ö., & Kilic, M. (2009). The Usage of IR Thermography for the Temperature Measurements Inside an Automobile Cabin. *International Communications in Heat and Mass Transfer*, *36*, 872-877.

[7] Astarita, T., Gardone, G., & Carlomango, G. M. (2006). Infrared thermography: an optical method in heat transfer and fluid flow visualization. *Optics and Lasers in Engineering, 44*, 261–281.

[8] Chevrette, P. (1986). Calibration of Thermal Imagers. Proceedings of the SPIE. *The International Society for Optical Engineering*, *661*, 372-382.

[9] Schwenn, T. (2008, July). *Discretization Primer and Modeling Discussion*. Presentation at RadTherm Training.

[10] Johnson, K., Curran, A., & Less, D. (1998). MuSES: A new heat and signature management design tool for virtual prototyping. *Proceedings of Ninth Annual Ground Target Modeling and Validation Conference*. Houghton, Michigan.

[11] Curran, A. R., Johnson, K., & Marttila, R. (1995).

Automated radiation modeling for vehicle thermal management. *SAE International Congress & Exposition*, *Underhood Thermal Management Session, Paper No. 950615*.
[12] Valisetty, R. R., Namburu, R. R., & Petit, G. (2004). Parallel MuSES for Infrared Signature Modeling of US Army Vehicles and Targets. *Army Research Laboratory ARL-TR*-328.
[13] Mayyas, A. (2010). *Comprehensive Thermal Modeling for Power Split Hybrid Power Train and Power Electronics*. Dissertation, Clemson University.
[14] Grujicic, M., Sellappan, V., & Omar, M. A. (2008). An Overview of the Polymer-to-Metal Direct-Adhesion Hybrid Technologies for Load-Bearing Automotive Components. *Journal of Materials Processing Technology*, *197*, 363-373.

Biographies

ABDELRAOUF MAYYAS is an Assistant Professor of Automotive Engineering at Arizona State University. He earned his B.S. degree from Mu'uta University, Jordan, MS Computer Engineering, 2006 from Yarmouk University, Jordan, and Ph.D. in Automotive Engineering, 2010 from Clemson University-International Center for Automotive Research "CU-ICAR", SC, USA. Dr. Mayyas is currently teaching at Arizona State University. His interests are in energy management control of hybrid electric vehicles, advanced propulsion systems and energy storage systems for renewable energy sources. Dr. Mayyas may be reached at amayyas@g.clemson.edu

MOHAMMAD OMAR is an Associate Professor of Mechanical Engineering at Clemson University. He earned his B.S. degree from University of Jordan, and Ph.D. Mechanical Engineering, 2005 from the University of Kentucky, USA. Dr. Omar is currently teaching at Clemson University-International Center for Automotive Research. His research interests are in the area of Manufacturing, Materials and Design; specifically, knowledge based manufacturing systems and light-weight design, non-destructive testing of materials and structures. His work is published in 5 book manuscripts, 4 US and Japanese Patents, and more than 90 refereed journal publications, conference proceedings and keynote presentations. Dr. Omar may be reached at momar@Clemson.edu.

PIERLUIGI PISU is an Assistant Professor of Electrical Engineering at Clemson University. He earned his M.S. (Computer Engineering1996) degree from University of Genoa, Italy, and Ph.D. (Electrical Engineering, 2002) from the Ohio State University. Dr. Pisu is currently teaching at Clemson University-International Center for Automotive Research CU-ICAR. His interests are in the model-based diagnostics and prognostics, modeling and control of hybrid electric vehicles, and energy storage systems. Dr. Pisu may be reached at Pisup@Clemson.edu.

A.M. KANNAN is an Associate Professor of Alternative Energy Technology at the Arizona State University. He earned his B.S. and M.S. from Madurai Kamaraj University (India) and Ph.D. (Fuel Cells, 1990) from the Indian Institute of Science, Bangalore, India. Dr. Kannan is teaching courses on Alternative Energy Technologies at the Arizona State University. His interests are fuel cells systems, advanced batteries and solar cells. Dr. Kannan may be reached at amk@asu.edu